

Transmission Electron Microscopy Tilt-Series Data from In-Situ Chondrocyte Primary Cilia

Michael J. Jennings¹, Timothy C. A. Molteno^{2,*}, Robert J. Walker³, Jennifer J. Bedford³, John P. Leader³ and Tony Poole³

¹ 4i Systems Ltd., 19 Warden Street, Opoho, Dunedin 9010, New Zealand; mike@4i.nz

² Department of Physics, University of Otago, P.O. Box 56, Dunedin 9016, New Zealand

³ Department of Medicine, University of Otago, P.O. Box 56, Dunedin 9016, New Zealand; rob.walker@otago.ac.nz (R.J.W.); jennifer.bedford@otago.ac.nz (J.J.B.); jhnlead8@hotmail.com (J.P.L.); tony.poole441@gmail.com (T.P.)

* Correspondence: tim@physics.otago.ac.nz

Abstract: The primary cilium has recently become the focus of intensive investigations into understanding the physical structure and processes of eukaryotic cells. This paper describes two tilt-series image datasets, acquired by transmission electron microscopy, of in situ chick-embryo sternal-cartilage primary cilia. These data have been released under an open-access licence, and are well suited to tomographic reconstruction and modelling of the cilium.

Dataset: doi:10.5281/zenodo.4592614.

Dataset License: CC BY-SA 4.0.

Keywords: primary cilia; electron tomography; TEM; chondrocyte; 3D reconstruction



Citation: Jennings, M.J.; Molteno, T.C.A.; Walker, R.J.; Bedford, J.J.; Leader, J.P.; Poole, T. Transmission Electron Microscopy Tilt-Series Data from In-Situ Chondrocyte Primary Cilia. *Data* **2021**, *6*, 118. <https://doi.org/10.3390/data6110118>

Academic Editor: Juraj Gregaň

Received: 1 October 2021

Accepted: 8 November 2021

Published: 15 November 2021

Publisher's Note: MDPI stays neutral with regard to jurisdictional claims in published maps and institutional affiliations.



Copyright: © 2021 by the authors. Licensee MDPI, Basel, Switzerland. This article is an open access article distributed under the terms and conditions of the Creative Commons Attribution (CC BY) license (<https://creativecommons.org/licenses/by/4.0/>).

1. Introduction

First identified in 1894 by Zimmermann [1], the primary cilium is a non-motile singular cytoplasmic organelle found in virtually all vertebrate cells. It has recently become the focus of intensive investigations into the physical structure and processes of eukaryotic cells [2–6]. The cilium is central to various pathways and modalities for signalling, allowing centrosomal processing and regulation of cellular and organelle function [7–9]. The enigmatic process of their nanoscale ciliogenesis and sensory function at present remain poorly understood [10]. Dysfunction of cilia or component proteins correlates with a wide spectrum of diseases, or ciliopathies, which express as developmental disorders and pathologies [11–14]. Whilst motile cilia have been intensively characterised [15,16], connective tissue primary cilia [4] and node cilia [17] have been comparatively less-well studied.

The first detailed nanometer-scale study of the three-dimensional anatomy of a chondrocyte primary cilium was carried out in 1978 [18] by exhaustive serial TEM imaging of ultrathin sections. Since then, electron tomography, or imaging biological structures using transmission electron microscopy (TEM) for 3D reconstruction, is widely used [3,19]. This allows for a greater detailed nanometer-scale spatial characterisation and modelling of structures with no loss of information due to sectioning [2,4,20,21]. These techniques involve imaging a sample through a series of tilt-angles in order to acquire data for later reconstruction into 3D volumes [22]. Some example TEM tilt-series images taken at different angles from the dataset described here are shown in Figure 1.

Previous 3D Reconstructions of Primary Cilia

Electron tomography from tilt-series data of portions of in situ chondrocyte primary cilia were first described in 2004 [3]. Full tomographic 3D reconstruction of an entire

cilium, from tilt-series data, was first published in 2012 [4,20]. Then in 2015, Shinohara et al. [17] published beautiful 3D reconstructions of the microtubules of murine node cilia. More recently with cryo-electron microscopy in vivo, Sun et al. [2] presented axoneme-architecture in IMCD3 cells, and Kiesel et al. [21] investigated the fine structures of cilia in MDCK-II cells. At the time of writing, no other TEM tilt-series datasets of in situ primary cilia are available in the public domain. This paper presents the TEM tilt-series dataset used for the original 3D reconstruction [4,20] of primary cilia. The data, as presented, are in a form that can easily be reconstructed in 3D using tools, such as IMOD [22].

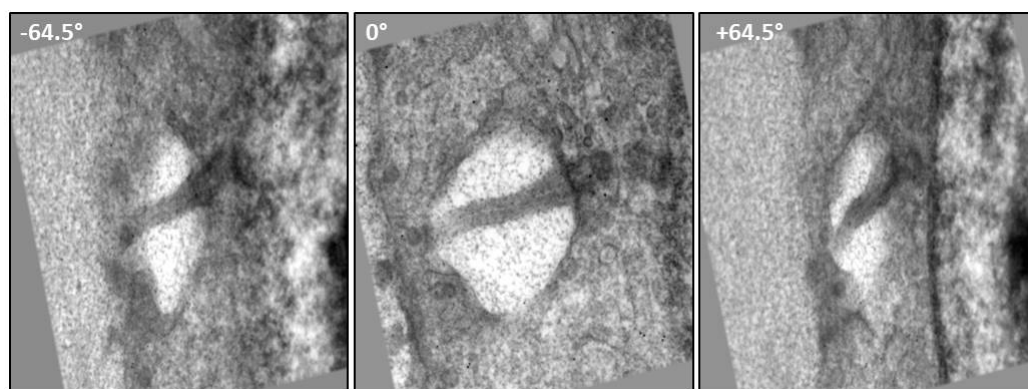


Figure 1. Data Acquisition: Raw single-axis TEM images from a tilt-series of a chick sternal chondrocyte primary cilium. The images shown were taken at angles of -64.50° , 0° and $+64.5^\circ$, respectively.

2. Materials and Methods

Domestic chicken (*Gallus domesticus*) embryonic sternal cartilage was chosen as a model tissue for chondrocyte cilia [6] for a number of reasons. The three cartilage vanes of the chick embryo sterna are easy to dissect, prepare, fix and embed for electron microscopy. The presence of low cell-numbers and a developing matrix allowed for smooth sectioning, providing excellent contrast and little obstruction for viewing between the extracellular matrix and the chondrocyte. Chondrocyte cilia appeared to be shorter and less deflected in their projections than those of other connective tissues, making chick embryonic sternal cartilage an ideal tissue model to investigate the relationships among the extracellular matrix, the primary cilium, the cytoskeleton and the Golgi apparatus [23].

2.1. Sample Preparation

Embryonic sternal cartilage was harvested after 15 days incubation at 39°C , and cut into 1 mm^3 pieces for embedding (producing tri-lateral segments). Samples were fixed in 2.5% glutaraldehyde with 1600 ppm ruthenium hexaamine tri-chloride (RHT) in 0.1 M sodium cacodylate buffer (pH 7.3) for 16 h at 37°C , and then post-fixed in 1% osmium tetroxide (OsO_4) with 1600 ppm RHT at 4°C for 4 h, followed by dehydration through a progressive series of graded ethanol concentrations (en bloc 4% uranyl acetate for 2 h in 50% ethanol). After transfer to propylene oxide, samples were embedded in EMBED-812 (ProSciTech, Kirwan, QLD, Australia) resin, oriented and left to polymerise in small rubber molds at 60°C for 24 h, as previously described by Poole et al. [6,24]. The RHT was added during the fixation process in order to retain extracellular matrix components [4,6,23–26].

2.1.1. Sectioning

Using optical microscopy resin-embedded specimens were selected for fixation quality, and then aligned with the block face parallel to the plane of the chondrocyte columns (see Figure 2). This was done as cilia preferentially align in this direction [27]. Resin blocks were sectioned into semithick (300–550 nm) sections with a Diatome™ diamond-knife on a Reichert Ultra-Microtome E (Reichert, Vienna, Austria). Serial sections were held together with formvar solution [28] before placement upon formvar-coated parallel-slot copper electron microscope grids. Investigative microscopy for candidate cilia was carried out

(100 kV on a Philips 410 electron microscope with a LaB₆ filament) at low beam currents to prevent aging and damage to the resin. Candidate cilia contained within the section and with good staining quality were selected as suitable for electron tomography. Some candidate cilia are shown in section Figure 2.

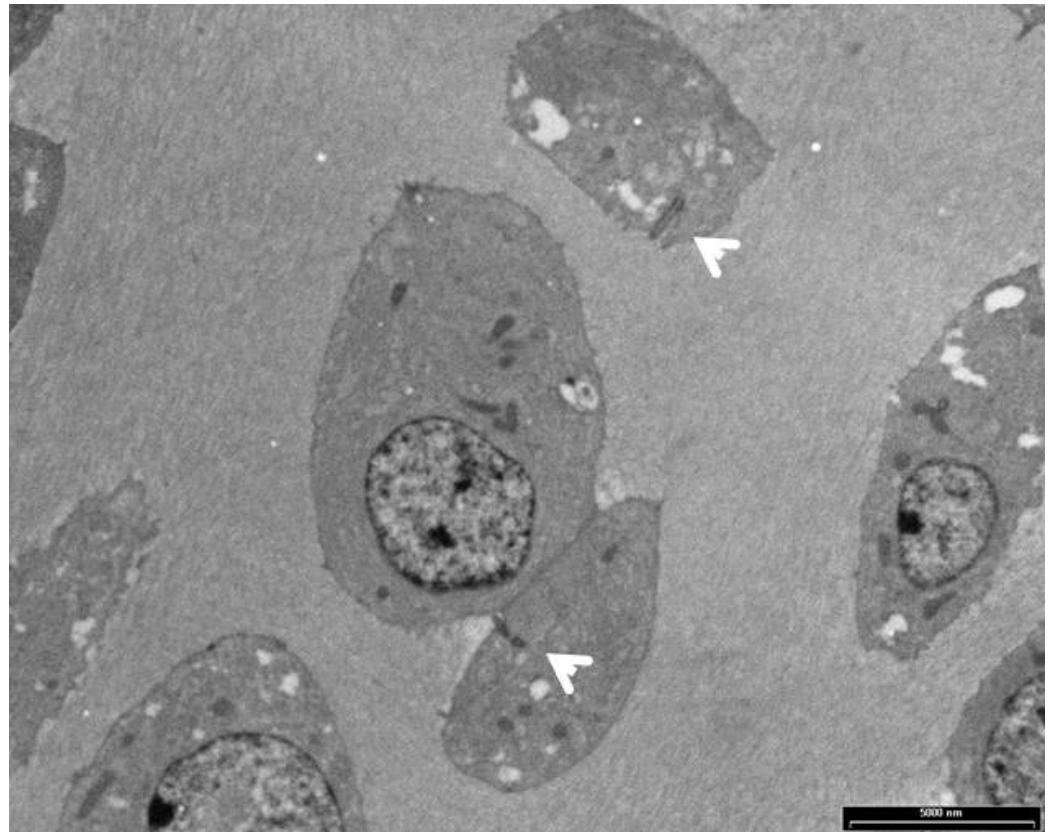


Figure 2. Chick embryo cartilage: A semithick section of chick embryo sternal cartilage detailing the extracellular matrix, chondrocytes and their primary cilia (arrowheads). Scale-bar 5 microns. Adapted from [4] with permission.

2.1.2. Fiducial Marking

Grids containing suitable candidate sections for tomography were labelled with 15 nm gold fiducial markers (British Bio-Cell, Cardiff, UK). Fiducials were applied to the top (resin section) and bottom (formvar) sides of the electron microscope grid, achieving a uniform distribution of 10–15 fiducials per square micron per side.

2.1.3. Tilt-Series Acquisition

The two samples were analysed using a FEI Tecnai G² F-30 transmission electron microscope (FEI Company, Hillsboro, OR, USA, with a LaB₆ filament electron source) at a 300 keV accelerating voltage. For both datasets, images were collected with a Tietz camera (2048 by 2048 pixels, 12-bit). The single-axis tilt-series was acquired using a tilt-holder at 85 different angles between -64.5° and $+64.5^\circ$ with increments of 1.5° . Full parameters for the single-axis dataset are shown in Table 1. The double axis tilt-series was acquired using a double tilt holder (GATAN Inc., Pleasanton, CA, USA). Each axis series was imaged over 121 angles between -60° and $+60^\circ$ with 1° increments. Full parameters for the double-axis dataset are shown in Table 2. Preview images from each dataset are shown in Figure 3.

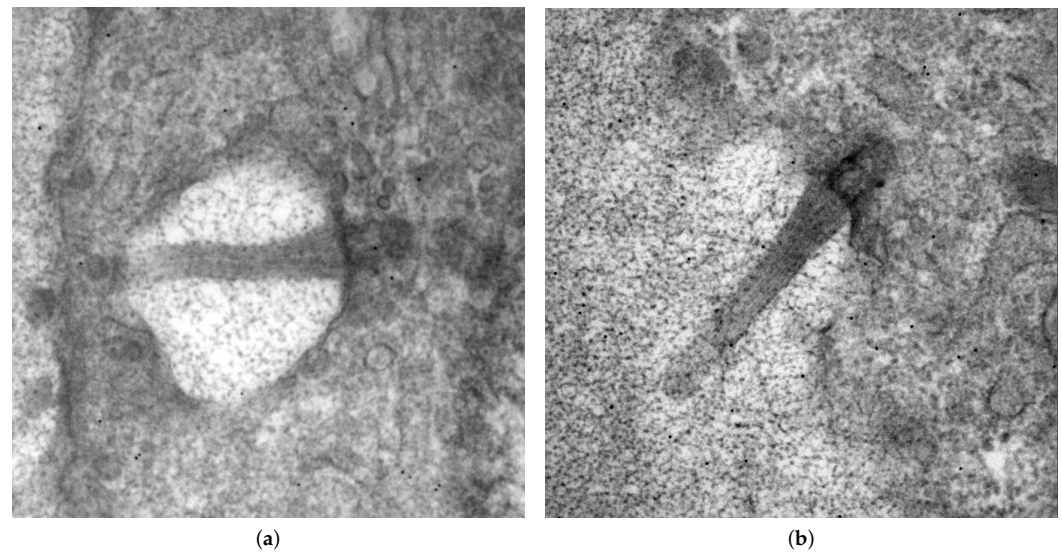


Figure 3. Preview images of the primary cilia examples from this dataset. Single-axis data are shown in (a) and dual-axis data in (b). Each primary cilium was contained within a 300 nm “semithick” section, from which tilt-series datasets were obtained.

Table 1. Tilt-series acquisition parameters from the single-axis dataset.

Parameter	Unit	Value
Max negative tilt	°	−64.50
Max positive tilt	°	64.50
Start tilt (skipping angles)	°	0.00
Relaxation Time	s	2.000
Tile scheme		Linear
Low tilt step	°	1.50
High tilt switch	°	50.00
High tilt step	°	1.50
Camera		CCD
(Initial) Exposure Time	s	1.00
Binning		1
Image pixel size	nm	1.21
Image area		(0, 0), (2048,2048)
Apply Corrections		None
Holder name		HT70_4
Optimized Position	μm	0.44
Tracking after (on) exposures		Yes
Tracking before exposures		No
Reference Image		Floating
Check Focus		−1
Periodicity (high tilt range)		1
Periodicity (low tilt range)		2
Periodicity switch angle		80.00
Applied Defocus	μm	−0.24
Tecnai Magnification		12,000
Tilt Axis Angle	°	11.18

Table 2. Tilt-series acquisition parameters from the dual-axis dataset. These data are contained within the .st acquisition files.

Parameter	Unit	Value
Max negative tilt	°	−60.00
Max positive tilt	°	60.00
Start tilt (skipping angles)	°	0.00
Tile scheme		Linear
Tilt step	°	1.0
Binning		1
Image pixel size	nm	1.21
Image area		(0, 0), (2048,2048)

3. Tilt-Series Dataset Description

This dataset consists of a TEMTomo_Dataset.7z archive containing two tilt-series folders: Single_Axis, a single axis tilt-series dataset and Dual_Axis, a dual axis tilt-series dataset (.mrc and .st) and their support .rawtlt and .txt files. Files consist of raw microscopy output data which are suitable for reconstruction in a number of software packages, such as IMOD [22]. The folder layout of the dataset is show in Figure 4.

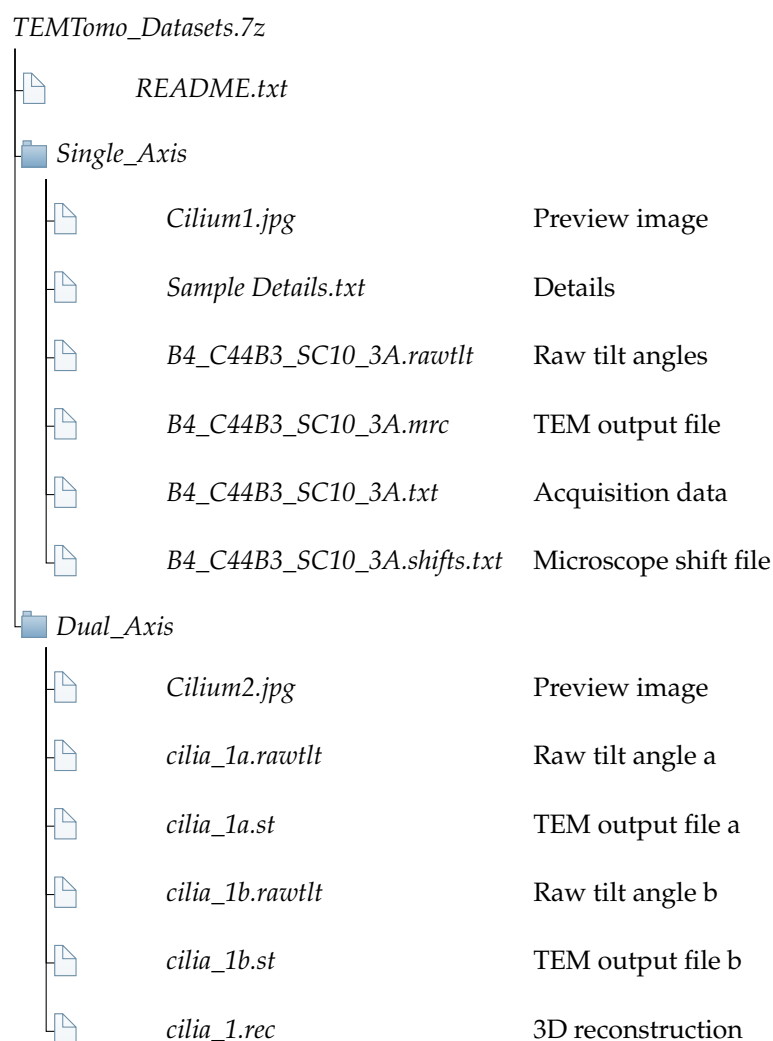
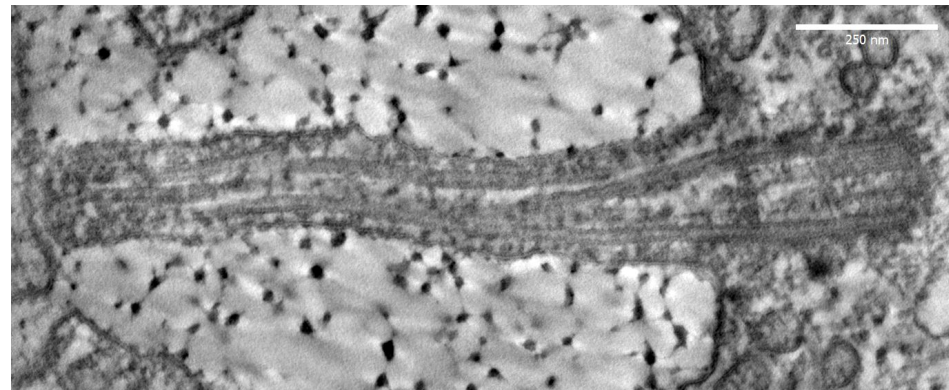


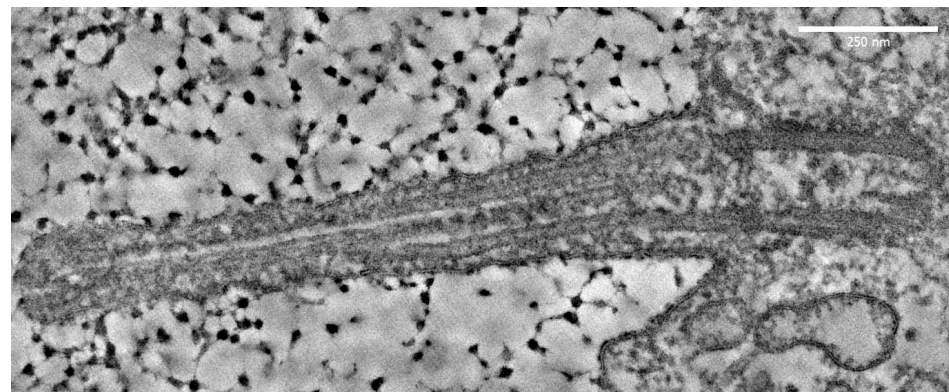
Figure 4. Directory structure of the tilt-series dataset archive.

4. Technical Validation

Both datasets were successfully 3D reconstructed using IMOD version 4.11.4. The reconstructed data are morphologically consistent with them describing primary cilia. The microtubule-doublet-based anatomy of the ciliary axoneme is shown in the reconstructed organelles projecting from the basal body (see Figure 5). This is consistent with the published morphology of connective tissue chondrocyte primary cilia [2,3,18]. The reconstructed axonemal lengths were 1.4 and 1.5 microns, respectively; and axoneme diameters decreased distally from 0.25 micron at the basal body, again consistent with published figures of Wilsman et al. [29] and Dummer et al. [30].



(a)



(b)

Figure 5. Longitudinal sections of reconstructed organelle ultrastructure showing the microtubule-doublet morphology characteristic of primary cilia. Single-axis Cilium1 is shown in (a) and dual-axis Cilium2 is shown in (b). Scale bars 250 nm.

Data Records

This dataset is available under the Creative Commons Attribution 4.0 International Public Licence at <https://doi.org/10.5281/zenodo.4592614> (accessed on 14 November 2021), and consists of an archive, TEMTomo_Dataset.7z, which contains two tilt-series TEM imaging datasets of primary cilia. The first dataset, in the folder *Single_Axis*, is a single axis tilt-series dataset, a preview of which is shown in Figure 5a. The second dataset, in the folder *Dual_Axis*, is a dual axis tilt-series dataset (see Figure 5b). Each folder contains raw unprocessed TEM output data files and associated support files containing tilt angles, and other parameters necessary for reconstruction. The folder layout of the dataset is shown in Figure 4.

5. Usage Notes

The tilt-series image datasets presented here can be reconstructed into tomograms by a number of software packages: UCSF [31], TomoJ [32], TOM [33] and IMOD [22]. We outline below the reconstruction procedure in IMOD. This closely follows the tutorial for the Etomo tool distributed as part of the IMOD package [34].

The reconstruction involves the following steps:

- Scanning headers and reading files.
- Coarse alignment of microscope tilt-series image data.
- Generate seed model.
- Aligning the stack.
- Fine alignment.
- Tomogram generation using back-projection.

Many of the required parameters are automatically loaded from headers by IMOD (e.g., image rotation and pixel size). The default values provided can be used for the majority of other parameters; however, those that differ from defaults are shown in Table 3. The resulting reconstruction is included in the dataset as the file `cilia_1.rec`.

Table 3. Selected parameters required for 3D reconstruction that differ from the default parameters in the etomo tool.

Parameter	Value
Fiducial Diameter	15 nm
Seed Points to select	25

6. Discussion and Conclusions

This paper presents two TEM tilt-series datasets of in situ primary cilia that were used for the original tomographic 3D reconstruction [4,20] of primary cilia. Notable in this dataset is the preservation of interconnected extracellular matrix granules, which interact directly with the axoneme and the ciliary membrane [3,6,23]. The data are suited for 3D reconstruction using tools such as IMOD [22]. By way of background for this work, the data were gathered to enable understanding of the three dimensional structure and function of the primary cilium. By releasing raw tilt-series data into the public domain, it is hoped that with potential improvements in reconstruction technology, the data may be useful for researchers investigating the structure and morphology of the primary cilium.

Author Contributions: Conceptualisation, M.J.J. and T.P.; methodology, M.J.J. and T.P.; validation, M.J.J.; formal analysis, M.J.J.; investigation, M.J.J.; resources, R.J.W. and T.P.; data curation, T.C.A.M.; writing—original draft preparation, M.J.J. and T.C.A.M.; writing—review and editing, M.J.J. and T.C.A.M.; visualisation, M.J.J. and T.C.A.M.; supervision, R.J.W., J.J.B., J.P.L. and T.P.; funding acquisition, M.J.J., T.P. and R.J.W. All authors have read and agreed to the published version of the manuscript.

Funding: This research was partially funded by a Kiwi Advanced Research and Education Network (KAREN), REANZ Network Capability Build Fund grant (2008).

Institutional Review Board Statement: The study was conducted according to the guidelines of the Declaration of Helsinki, and approved by the Ethics Committee of the University of Otago (protocol code 09/111).

Informed Consent Statement: Not applicable.

Data Availability Statement: This dataset is available at <https://doi.org/10.5281/zenodo.4592614> (accessed on 14 November 2021).

Acknowledgments: I would like to thank Allan Mitchell, Richard Easingwood, Gillian Grayston, Katrin Geist and Duane Harland, for their kind assistance regarding electron microscopy techniques; and David Mastronarde of Boulder Colorado for their tireless support with the IMOD software packages. I would also like to thank Irina Alieva for her fundamental insight into the primary cilium.

Conflicts of Interest: The authors declare no conflict of interest.

Abbreviations

The following abbreviations are used in this manuscript:

TEM	Transmission Electron Microscopy
RHT	Ruthenium Hexamine Trichloride
3D	Three Dimensional
IMCD	Inner Medullary Collecting Duct
MDCK	Madin-Darby Canine Kidney

References

- Zimmermann, K. Demonstration: Plastische reconstruction des hirnrohres; Schnittserie, Kaninchenembryo; Photogramm; Präparate von Uterus, Nebenhoden, Darm, Ureter, Niere, Thranendrüse. *Verhandlungen der Anatomischen Gesellschaft auf der achten Versammlung zu Strassburg, vom 13–16 Mai 1894*, *8*, 244–245.
- Sun, S.; Fisher, R.L.; Bowser, S.S.; Pentecost, B.T.; Sui, H. Three-dimensional architecture of epithelial primary cilia. *Proc. Natl. Acad. Sci. USA* **2019**, *116*, 9370–9379. [[CrossRef](#)]
- Jensen, C.G.; Poole, C.A.; McGlashan, S.R.; Marko, M.; Issa, Z.I.; Vujcich, K.V.; Bowser, S.S. Ultrastructural, tomographic and confocal imaging of the chondrocyte primary cilium in situ. *Cell Biol. Int.* **2004**, *28*, 101–110. [[CrossRef](#)] [[PubMed](#)]
- Jennings, M.J. Ultrastructural Modelling of the Matrix-Cilium-Golgi Continuum in Hyaline Chondrocytes. Ph.D. Thesis, University of Otago, Dunedin, New Zealand, 2015. [[CrossRef](#)]
- Satir, P.; Pedersen, L.B.; Christensen, S.T. The primary cilium at a glance. *J. Cell Sci.* **2010**, *123*, 499–503. [[CrossRef](#)]
- Poole, C.A.; Flint, M.H.; Beaumont, B.W. Analysis of the morphology and function of primary cilia in connective tissues: A cellular cybernetic probe? *Cell Motil.* **1985**, *5*, 175–193. [[CrossRef](#)]
- Alieva, I.B.; Uzbekov, R.E. The centrosome is a polyfunctional multiprotein cell complex. *Biochemistry* **2008**, *73*, 626–643. [[CrossRef](#)]
- Kwon, O.S.; Mishra, R.; Safieddine, A.; Coleno, E.; Alasseur, Q.; Faucourt, M.; Barbosa, I.; Bertrand, E.; Spassky, N.; Le Hir, H. Exon Junction Complex dependent mRNA localization is linked to centrosome organization during ciliogenesis. *Nat. Commun.* **2021**, *12*, 1351. [[CrossRef](#)] [[PubMed](#)]
- Takacs, Z.; Proikas-Cezanne, T. Primary cilia mechanosensing triggers autophagy-regulated cell volume control. *Nat. Cell Biol.* **2016**, *18*, 591–592. [[CrossRef](#)] [[PubMed](#)]
- Yoon, J.; Commerci, C.J.; Weiss, L.E.; Milenkovic, L.; Stearns, T.; Moerner, W. Revealing nanoscale morphology of the primary cilium using super-resolution fluorescence microscopy. *Biophys. J.* **2019**, *116*, 319–329. [[CrossRef](#)]
- Stayner, C.; Poole, C.A.; McGlashan, S.R.; Pihanathanond, M.; Brauning, R.; Markie, D.; Lett, B.; Slobbe, L.; Chae, A.; Johnstone, A.C.; et al. An ovine hepatorenal fibrocystic model of a Meckel-like syndrome associated with dysmorphic primary cilia and TMEM67 mutations. *Sci. Rep.* **2017**, *7*, 1601. [[CrossRef](#)]
- Lee, J.; Park, K.C.; Sul, H.J.; Hong, H.J.; Kim, K.H.; Kero, J.; Shong, M. Loss of primary cilia promotes mitochondria-dependent apoptosis in thyroid cancer. *Sci. Rep.* **2021**, *11*, 4181. [[CrossRef](#)]
- Patel, H.; Li, J.; Herrero, A.; Kroboth, J.; Byron, A.; Von Kriegsheim, A.; Brunton, V.; Carragher, N.; Hurd, T.; Frame, M. Novel roles of PRK1 and PRK2 in cilia and cancer biology. *Sci. Rep.* **2020**, *10*, 3902. [[CrossRef](#)]
- Shamseldin, H.E.; Shaheen, R.; Ewida, N.; Bubshait, D.K.; Alkuraya, H.; Almardawi, E.; Howaidi, A.; Sabr, Y.; Abdalla, E.M.; Alfaifi, A.Y.; et al. The morbid genome of ciliopathies: An update. *Genet. Med.* **2020**, *22*, 1051–1060. [[CrossRef](#)]
- Fisch, C.; Dupuis-Williams, P. Ultrastructure of cilia and flagella—back to the future! *Biol. Cell* **2011**, *103*, 249–270. [[CrossRef](#)]
- Satir, P. CILIA: Before and after. *Cilia* **2017**, *6*, 1. [[CrossRef](#)]
- Shinohara, K.; Chen, D.; Nishida, T.; Misaki, K.; Yonemura, S.; Hamada, H. Absence of radial spokes in mouse node cilia is required for rotational movement but confers ultrastructural instability as a trade-off. *Dev. Cell* **2015**, *35*, 236–246. [[CrossRef](#)] [[PubMed](#)]
- Wilsman, N.J. Cilia of adult canine articular chondrocytes. *J. Ultrastruct. Res.* **1978**, *64*, 270–281. [[CrossRef](#)]
- De Rosier, D.; Klug, A. Reconstruction of three dimensional structures from electron micrographs. *Nature* **1968**, *217*, 130–134. [[CrossRef](#)]
- Poole, C.A.; Jennings, M.J.; Walker, R.J. Modeling the Matrix-Cilium-Golgi continuum in hyaline chondrocytes by electron tomography. *Cilia* **2012**, *1*, P39. [[CrossRef](#)]
- Kiesel, P.; Viar, G.A.; Tsoy, N.; Maraspini, R.; Gorilak, P.; Varga, V.; Honigmann, A.; Pigino, G. The molecular structure of mammalian primary cilia revealed by cryo-electron tomography. *Nat. Struct. Mol. Biol.* **2020**, *27*, 1115–1124. [[CrossRef](#)]

22. Kremer, J.R.; Mastronarde, D.N.; McIntosh, J.R. Computer visualization of three-dimensional image data using IMOD. *J. Struct. Biol.* **1996**, *116*, 71–76. [[CrossRef](#)]
23. Poole, C.A.; Zhang, Z.J.; Ross, J.M. The differential distribution of acetylated and deetyrosinated alpha-tubulin in the microtubular cytoskeleton and primary cilia of hyaline cartilage chondrocytes. *J. Anat.* **2001**, *199*, 393–405. [[CrossRef](#)] [[PubMed](#)]
24. Poole, C.A.; Reilly, H.C.; Flint, M.H. The adverse effects of HEPES, TES, and BES zwitterion buffers on the ultrastructure of cultured chick embryo epiphyseal chondrocytes. *In Vitro* **1982**, *18*, 755–765. [[CrossRef](#)]
25. Luft, J.H. Ruthenium red and violet. I. Chemistry, purification, methods of use for electron microscopy and mechanism of action. *Anat. Rec.* **1971**, *171*, 347–368. [[CrossRef](#)] [[PubMed](#)]
26. Luft, J.H. Ruthenium red and violet. II. Fine structural localization in animal tissues. *Anat. Rec.* **1971**, *171*, 369–415. [[CrossRef](#)]
27. Farnum, C.E.; Wilsman, N.J. Orientation of primary cilia of articular chondrocytes in three-dimensional space. *Anat. Rec. Adv. Integr. Anat. Evol. Biol.* **2011**, *294*, 533–549. [[CrossRef](#)] [[PubMed](#)]
28. Sawyer, L.; Grubb, D.T.; Meyers, G.F. *Polymer Microscopy*; Springer Science & Business Media: New York, NY, USA, 2008.
29. Wilsman, N.J.; Fletcher, T.F. Cilia of neonatal articular chondrocytes incidence and morphology. *Anat. Rec.* **1978**, *190*, 871–889. [[CrossRef](#)] [[PubMed](#)]
30. Dummer, A.; Poelma, C.; DeRuiter, M.C.; Goumans, M.J.T.; Hierck, B.P. Measuring the primary cilium length: Improved method for unbiased high-throughput analysis. *Cilia* **2016**, *5*, 7. [[CrossRef](#)]
31. Zheng, S.Q.; Sedat, J.; Agard, D. Automated data collection for electron microscopic tomography. *Methods Enzymol.* **2010**, *481*, 283–315. [[PubMed](#)]
32. Messaoudi, C.; Boudier, T.; Sorzano, C.O.S.; Marco, S. TomoJ: Tomography software for three-dimensional reconstruction in transmission electron microscopy. *BMC Bioinform.* **2007**, *8*, 288. [[CrossRef](#)]
33. Nickell, S.; Förster, F.; Linaroudis, A.; Del Net, W.; Beck, F.; Hegerl, R.; Baumeister, W.; Plitzko, J.M. TOM software toolbox: Acquisition and analysis for electron tomography. *J. Struct. Biol.* **2005**, *149*, 227–234. [[CrossRef](#)] [[PubMed](#)]
34. Gaudette, R.; Mastronarde, D. Using Etomo. 2021. Available online: <https://bio3d.colorado.edu/imod/doc/UsingEtomo.html> (accessed on 26 March 2021).